J Sol-Gel Sci Technol (2015) 76:180–194
DOI 10.1007/s10971-015-3765-6

ORIGINAL PAPER

Enhanced photocatalytic activity of mesoporous SiO_2/TiO_2 sol–gel coatings doped with Ag nanoparticles

M. V. Roldán[1] · Y. Castro[2] · N. Pellegri[1] · A. Durán[2]

Received: 10 February 2015 / Accepted: 5 June 2015 / Published online: 16 June 2015

Abstract In the present study, as-prepared silver nanoparticles have been incorporated into SiO_2 and TiO_2 sols. The characterisation of the silver nanoparticles was performed through transmission electron microscopy, grazing X-ray diffraction, and UV–visible spectroscopy, before and after mixing with the different sols. Multilayer coatings doped with silver nanoparticles were also prepared by combining different compositions and analysed by TEM and GXRD. The photocatalytic activity was studied through the degradation of methyl orange in aqueous solution under UV light exposure. High photocatalytic efficiency was observed for all the multilayer coatings. The highest efficiency was obtained for the Ag–SiO_2/TiO_2 mesoporous system that reached a degradation percentage of methyl orange up to 94 % after 2.5 h of irradiation, near the complete elimination of the pollutant. The mechanism that explains the high photocatalytic efficiency of this multilayer coating is associated with the high porosity of the mesoporous coatings and with the increase in the local electric field, associated with the effect of plasmon resonance surface produced for the presence of metallic silver nanoparticles in the SiO_2 film.

✉ Y. Castro
castro@icv.csic.es

[1] Laboratorio de Materiales Cerámicos, Facultad de Ciencias Exactas, Ingeniería y Agrimensura, Instituto de Física Rosario-Consejo Nacional de Investigaciones Científicas y Técnicas, Universidad Nacional de Rosario, Pellegrini 250, 2000 Rosario, Argentina

[2] Instituto de Cerámica y Vidrio (Consejo Superior de Investigaciones Científicas), Campus de Cantoblanco, 28049 Madrid, Spain

Graphical Abstract

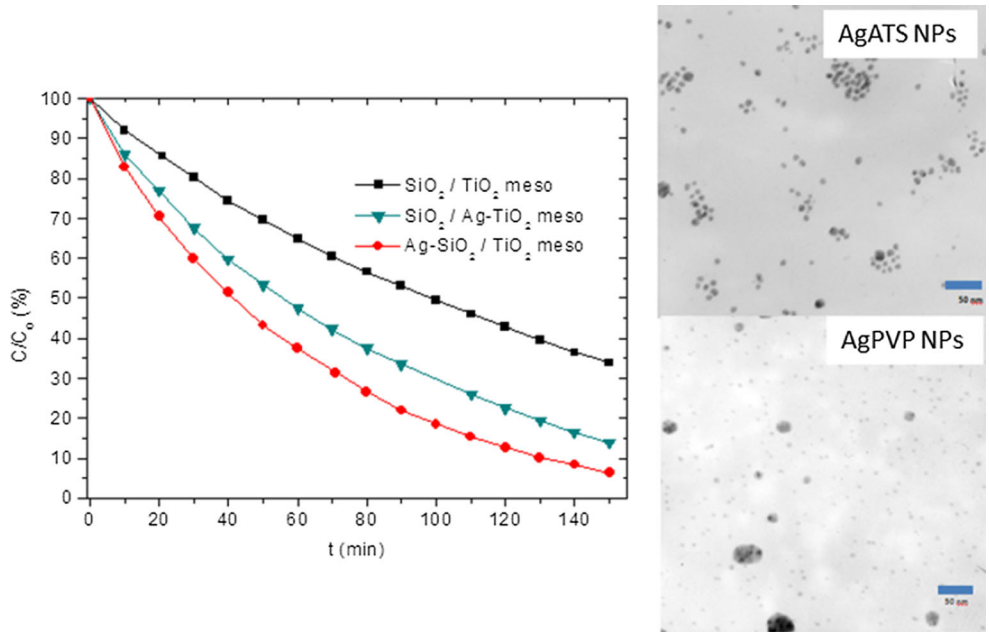

Keywords Ag nanoparticles · Mesoporous films · Sol–gel · TiO_2 · Photocatalysis · Semiconductors

1 Introduction

Semiconductor materials are extensively studied due to their great variety of applications [1]. Titania (TiO_2) is one of the most interesting materials for decontamination, purification, and deodorisation of air and water [2, 3], because its photocatalytic activity permits the degradation of harmful organic contaminants. The bactericide properties of titania complement this functionality [4]. Other valuable characteristics such as an excellent optical transparency in the visible and near-infrared regions, high corrosion resistance, chemical and thermal stability, and low cost [5] make it a suitable material for indoor purification: office buildings, self-sterilising surfaces, food and cosmetic industries or ambient in industrial work environments [6–9].

The photocatalytic degradation process induced by TiO_2 is based on the semiconductor activation by UV and/or visible light irradiation with the subsequent generation of electron–hole pairs. These pairs diffuse to the titania surface, reacting with adsorbed water, hydroxyl groups, and molecular oxygen, producing active radicals which react with the organic compounds. The photocatalytic activity mainly depends on the redox potential of the surface and on the lifetime of electron–hole pairs. In order to improve the reaction rate and the efficiency of the photocatalyst, different strategies have been considered, including manipulation of the crystal structure [10], generation of vacancies [11], doping with other elements [12], functionalisation of the interface [13], and increase in surface area [14], among others.

Many of these approaches have been applied to photocatalytic powders [15]. However, the main disadvantage of using powder is the necessary separation of photocatalyst particles after treatment, [16]. The immobilisation of TiO_2 on transparent substrates is a highly promising alternative to prevent this problem. Moreover, transparent thin films are already used in self-cleaning windows for buildings [17]. Different techniques, such as spray pyrolysis [18], sol–gel method [14, 19], sputtering [20], solvothermal method [21], pulsed laser deposition [22], atomic layer deposition [23], and chemical vapour deposition (CVD) [24], have been used to obtain TiO_2 coatings. Particularly, sol–gel process is widely used due to its multiple advantages, including the easiness to obtain TiO_2 in anatase phase at low temperature. This technique allows obtaining homogeneous, transparent, scratch-resistant, and well-adhered TiO_2 thin films which cannot be attained by other methods such as the doctor-blade technique from commercial TiO_2 as Degussa's P25 [25]. As additional advantage, the sol–gel technique allows tuning the thickness of the thin films over a wide range of values, and to combine different oxides in multilayer systems. Moreover, the design and development of mesostructured TiO_2 materials by combining the sol–gel method with the use of surfactants as structure-directing agents allow producing coatings with tailored pore sizes and high specific surface area. The contact surface between the catalyst and the

species to be eliminated greatly increases in these films, improving their photocatalytic activity [14, 26] compared to that of powder and bulk materials. These characteristics allow solving the limitations on the pore size of zeolites and provide new opportunities in catalytic applications.

On the other hand, the development of materials with metallic nanoparticles has gained great attention in material science [27, 28]. Particularly, silver nanoparticles are considered an attractive noble metal due to their outstanding catalytic, electric, and optical properties. The modification of TiO_2 anatase coatings with silver nanoparticles can change the surroundings of TiO_2 and modify the photocatalytic properties, improving the separation efficiency of the photo-generated electron–hole pairs and increasing the efficiency of charge carrier's transfer to the surrounding supports [29–31], among other mechanisms. Consequently, the combination of TiO_2 and silver nanoparticles appears as an alternative and innovative photocatalyst with further bactericide properties [32].

Different processing methods have been reported for preparing TiO_2 materials doped with silver nanoparticles. Several authors describe the infiltration of TiO_2 coatings with silver salts from aqueous solution followed by a treatment to reduce Ag^+ ions, such as UV irradiation [33] or chemical reduction [34]. However, these procedures tend to accumulate the metal nanoparticles on the surface of the film. Thus, silver nanoparticles are exposed to the surrounding medium, and oxidation [35] and/or dissolution [36] might occur, reducing the lifetime of the material. Other authors incorporate silver salts, mainly nitrates and chlorides, into the TiO_2 sol [30, 37, 38]. During the heat treatment, several mechanisms take place for reducing Ag^+ ions into Ag^0. The nanoparticles are not necessarily uniform in size; moreover, the size difference between Ti^{4+} and Ag^+ causes the migration of silver ions to the TiO_2 surface during the heat treatment, also resulting in the metal deposition on the TiO_2 surface by calcination [38].

Thus, the ex situ synthesis of metallic nanoparticle suspensions further incorporated to sol–gel sols in two-step synthesis processes might overcome these limitations allowing to obtain stable and homogeneous solutions able to prepare transparent coatings.

Different methods have been employed to prepare shape- and size-controlled suspensions of silver nanoparticles [39], including chemical reduction of silver salts in solution [40–42], thermal decomposition in organic solvents [43], biochemical reduction [44], chemical and photo-reduction in reverse micelles [45], 'nanosphere lithography' (NSL) [46], electrochemical reduction [47, 48], photo-reduction [49], and microwave-assisted techniques [50]. Each method has typical advantages and disadvantages. Chemical reduction in solution is a simple method which allows obtaining stable colloidal silver nanoparticles in ethanol, which is the solvent used for the present sol–gel synthesis. Consequently, this technique appears as the most adequate choice to synthesise silver nanoparticles according to our objectives.

The objective of this work was to prepare TiO_2 and SiO_2 coatings doped with silver nanoparticles homogeneously dispersed and with controlled size by adding colloidal silver nanoparticles obtained ex situ to silica and titania sols. During sol–gel process, hydrolysis and condensation reactions will occur around the silver nanoparticles, which results in their embedding in SiO_2 or TiO_2 coatings.

We have selected an effective method to incorporate Ag-NPs reported in [42, 51] to the synthesis of SiO_2 and TiO_2 sols for obtaining Ag–SiO_2 and dense and mesoporous Ag–TiO_2 coatings by sol–gel. Moreover, the incorporation of Ag-NPs suspensions to the sols was optimised to ensure a homogeneous distribution of the nanoparticles in the coatings, thus avoiding the agglomeration of the nanoparticles in the TiO_2 surface and their possible dissolution as previously reported.

The photocatalytic behaviour of different multilayer structures combining Ag-NP-doped layers of SiO_2 and TiO_2 was studied through degradation of methyl orange (MO) under UV excitation, showing an extremely high efficiency. The possible mechanisms ruling this enhanced efficiency are discussed and correlated with the synthesis processes.

In one previous work [52], we found a clear relationship between the architecture of the multilayer coatings and the photocatalytic and bactericide behaviour. The aim of this work was to study the influence of the parameters involved in the synthesis of TiO_2 sols doped with Ag-NPs along with the effect of different SiO_2/TiO_2 coating architectures on the photocatalytic efficiency of the systems. Up to our knowledge, this is the first time that a complete characterisation step by step of the synthesis process is shown and further related with the film properties. These results will contribute to the available knowledge for the rational design of novel functional materials and to identify suitable synthesis conditions that allow obtaining a high enhancement of the photocatalytic efficiency of SiO_2/TiO_2 coatings.

2 Experimental

Reactives Ethanol absolute (EtOH, Panreac); silver nitrate ($AgNO_3$, Merck); *N*-(3-trimethoxysilylpropyl)diethylenetriamine (ATS, Aldrich); polyvinylpyrrolidone (PVP, Aldrich); tetraethyl orthosilicate (TEOS, ABCR); titanium isopropoxide (TISP, ABCR); acetic acid (AcOH, Panreac); $(polyethyleneglycol)_{20}$ hexadecyl ether (Brij58, Sigma); deionised water (H_2O, Panreac); hydrochloric acid (HCl, Merck).

2.1 Preparation of silver nanoparticles

Aminosilane-stabilised Ag nanoparticles (Ag-ATS) were prepared by a colloidal method following the process previously described [42, 51]. Silver nitrate was dissolved in ethanol under ultrasound stirring and mixed with ATS in ethanol under N_2 atmosphere with final ratios equal to 12 mM $AgNO_3$ and 62.5 mM ATS. The final solution was mixed and homogenised by mechanical stirring and kept at 40 °C for 8 h under N_2 atmosphere. A yellow solution was obtained, the colour being indicative of the formation of silver nanoparticles [53, 54]. The Ag-ATS colloidal suspension was stored in darkness at room temperature.

On the other hand, silver nanoparticles were also obtained by stabilisation with polyvinylpyrrolidone (Ag-PVP) following a similar procedure. A homogeneous solution of 12 mM $AgNO_3$ and 60 mM PVP was prepared in absolute ethanol and kept at 70 °C for 4 h with magnetic stirring. An orange solution was obtained associated with the higher final concentration of silver nanoparticles. The Ag-PVP colloidal suspension was also stored in darkness at room temperature.

2.2 Characterisation of Ag nanoparticles

The Ag-ATS and Ag-PVP colloidal suspensions were characterised by transmission electronic microscopy (TEM, Hitachi H-7100 equipment). TEM samples were obtained by depositing a drop of the suspension onto carbon-coated copper grids. The mean size was calculated measuring more than 100 particles over several images using the ImageJ software. The particle size was also measured by dynamic light scattering (DLS) with a Zetasizer Nanor ZS (Malvern) equipment. UV–Visible spectra of Ag-ATS and Ag-PVP colloidal suspensions were recorded with PerkinElmer (Lambda 950) equipment working in direct transmittance mode. To characterise the crystalline structure, grazing incident X-ray diffraction (GXRD) patterns were obtained with CuK_α radiation in a PANalytical diffractometer (X'pert PRO theta/theta) in the range $2\theta = 20°–70°$, with a counting time of 20 s/step, an incidence angle of 0.5° and an increment of 0.05°. The samples were prepared depositing a drop of each suspension of silver nanoparticles on Si wafers and allowed to evaporate at room conditions.

2.3 Preparation of sol–gel sols

2.3.1 SiO_2 sol

The SiO_2 sol was obtained in two steps. First, TEOS was dissolved in EtOH, and HCl 0.1 N was added dropwise up to a molar ratio of 1 TEOS:12 EtOH:1 H_2O. The sol was refluxed at 60 °C for 90 min. In the second step, HCl 0.1 N was added up to a final molar ratio of 1 TEOS:4 H_2O. The final solution was maintained under reflux at 40 °C for 90 min.

2.3.2 Ag-doped SiO_2 suspension

First, SiO_2 sol was prepared by mixing TEOS with EtOH and adding HCl 0.1 N under stirring. After refluxed at 70 °C for 8 h, a transparent sol was obtained with a molar ratio of 1 TEOS:3.6 EtOH:1.4 H_2O. Then, this SiO_2 sol was mixed with the previously obtained Ag-ATS suspension, added dropwise under continuous agitation. The Ag-doped SiO_2 suspension was further homogenised and concentrated using a rotary evaporator until achieving a concentration of 0.4 M SiO_2 and 0.038 M Ag-ATS sol.

2.3.3 TiO_2 sol

TiO_2 sol was obtained by mixing TISP with AcOH in a molar ratio TISP/AcOH = 1 and adding together absolute ethanol. The sol was maintained 1 h under stirring to form a chelate that allowed controlling the hydrolysis and condensation reactions. The remaining ethanol was mixed with acidulated water (0.1 N HCl) and added drop by drop to the first solution. The molar ratio of the final sol was 1 TISP:1 AcOH:40 EtOH:2 H_2O, and TiO_2 concentration was fixed as 30 g/L. The sol was aged for 2 days before using.

To obtain mesoporous films, TiO_2-Brij58 sol was prepared following a similar process, but incorporating Brij58 as poro-generating agent in a molar ratio of 1 TISP:0.07 Brij58 to TiO_2 sol [26].

2.3.4 Ag-doped TiO_2 suspension

Ag-doped TiO_2 suspensions were prepared using PVP-stabilised silver nanoparticles (Ag-PVP). The suspensions were obtained by mixing the corresponding TiO_2 sol with the Ag-PVP colloidal suspension added dropwise up to a concentration of 0.09 M TiO_2 and 9 mM Ag-PVP; it was after homogenised and concentrated up to a final concentration of 0.37 M TiO_2 and 0.037 M Ag-PVP.

2.4 Characterisation of Ag-doped SiO_2 and Ag-doped TiO_2 suspensions

The Ag–SiO_2 and Ag–TiO_2 suspensions were characterised by UV–Visible spectroscopy to identify the presence of Ag-NPs. The stability of the suspensions was assessed through the evolution of viscosity with time, using a vibrational viscometer (SV 1A, A&D Company). GXRD patterns were performed with CuK_α radiation in the range $2\theta = 20°–70°$, with a counting time of 20 s/step, an

Table 1 Composition, refractive index, thickness, pore volume, and roughness of the coatings

Coating samples	Composition	Refractive index ±0.05 (λ = 700 nm)	Thickness (nm) ±2	V_{porous} (%)	Surface roughness RMS (nm)
SiO_2/TiO_2 dense	1 layer of SiO_2 sol	1.44	210	–	1.6
	2 layers of TiO_2 sol	2.09	90	–	
SiO_2/TiO_2 meso	1 layer of SiO_2 sol	1.44	210	–	2.7
	2 layers of TiO_2-Brij58 sol	1.73	140	25	
Ag–SiO_2	1 layer of Ag-doped SiO_2 suspension	1.43	380	7	2.1
Ag–SiO_2/TiO_2 dense	1 layer of Ag-doped SiO_2 suspension	1.43	380	7	5.0
	2 layers of TiO_2 sol	2.09	170	–	
Ag–SiO_2/TiO_2 meso	1 layer of Ag-doped SiO_2 suspension	1.43	380	7	6.6
	2 layers of TiO_2-Brij58 sol	1.73	280	25	
SiO_2/Ag–TiO_2 dense	1 layer of SiO_2 sol	1.44	210	–	5.8
	2 layers of Ag-doped TiO_2 suspension	1.80	290	12	
SiO_2/Ag–TiO_2 meso	1 layer of SiO_2 sol	1.44	210	–	4.3
	2 layers of Ag-doped TiO_2-Brij58 suspension	1.68	300	29	

incidence angle of 0.5°, and an increment of 0.05° to identify the crystallisation and oxidation state of Ag-NPs. The samples were prepared depositing a drop of each suspension on Si wafers and allowed to evaporate at room conditions.

2.5 Deposition of the coatings

Coatings were deposited on soda lime glass slides from the different sols by dip-coating at constant extraction rates [55]. Some films were also obtained on Si wafers and quartz glass.

All the systems studied consist on one first SiO_2 layer followed by two layers of dense or mesoporous TiO_2. After each dipping process, the corresponding heat treatment was performed. The SiO_2 layer has the main function of acting as physical barrier against diffusion of Na^+ ions from soda lime glass slides to the TiO_2 layer that would poison the semiconductor inhibiting the photocatalytic activity [56]. SiO_2 layer can also act as physical medium to incorporate silver nanoparticles. In this way, it was possible to obtain different two-layer architectures incorporating silver nanoparticles in the inner SiO_2 film or in the outer layer of TiO_2. Different multilayer systems were prepared to study the reactivity, stability, and functionality. Samples without silver nanoparticles were prepared as references, to be compared with the corresponding Ag-doped samples for studying the effect of silver nanoparticles in the photocatalytic behaviour.

SiO_2 and Ag-doped SiO_2 layers were deposited by dip-coating at 25 cm/min and 35 cm/min, respectively, and heat treated at 450 °C for 30 min.

Dense and mesoporous TiO_2 layers and multilayers were deposited on Si wafers, quartz glass, and soda lime glass slides using TiO_2 and TiO_2-Brij58 sols at 25 and 35 cm/min, respectively, at a relative humidity of 20 %. In the case of multilayers, an intermediate heat treatment was performed at 350 °C for 1 h with a heating rate of 10 °C/min, followed by a final sintering at 450 °C for 1 h using the same heating rate. Ag–TiO_2 and Ag–mesoporous TiO_2 layers and multilayers were deposited following the same procedure.

Table 1 summarises the seven multilayer coating structures built by combining the different sol compositions. A graphical scheme of the coatings is presented in [51].

2.6 Characterisation of the coatings

FTIR spectra of Ag–SiO_2, dense Ag–TiO_2, and mesoporous Ag–TiO_2 monolayer coatings on Si wafers were obtained in transmission mode with PerkinElmer FTIR Spectrum 100 equipment in the range of 4000–400 cm^{-1} with a resolution of 2 cm^{-1}. GXRD measurements (range 2θ = 20°–70°, fixed time of 20 s/step, and increments of 0.05°) were also taken on the same coatings. The structure characterisation of the coatings was studied by TEM.

Thickness (e) and refractive index (n) were measured using a Spectroscopic Ellipsometer [WVASE32 ('Variable Angle Spectroscopic Ellipsometer') J.A. Co., Woollam M-2000UTM]. The pore volume of the films was determined using the Bruggeman effective medium approximation (BEMA) [57].

Photoluminescence emission spectra (PL) of photocatalytic samples were performed to take light on the mechanism of photo-assisted reactions. Spectra were recorded by Shimadzu RF-5301PC spectrofluorophotometer with a Xe lamp, adjusting the excitation wavelength at 280 nm.

UV–Vis absorption spectra of Ag-doped and non-doped TiO_2 monolayers deposited on quartz were recorded using a Jasco V-530 equipment in the range of 200–1100 nm. Band gap values were determined using the Eq. (1).

$$(\alpha E)^{1/m} = A\left(E - E_g\right) \quad (1)$$

where α is the absorption coefficient, E_g is the band gap energy, E is the energy of the incident photon, A is a constant, and m is a parameter that depends on the electronic transition of the semiconductor; for indirect transition semiconductor such as TiO_2 anatase phase, $m = 2$ [58].

2.7 Photocatalytic tests

Photocatalytic properties of the multilayer systems (Table 1) were studied through the degradation of MO in aqueous solution. The measurements were taken using 50 mL of an aqueous solution of MO with a concentration of 3 mg/L at pH = 2 and a total surface tested equal to 50 cm^2, corresponding to four coated samples. The container was covered with window glass to avoid evaporation and maintained under stirring during the entire test. The system was irradiated from the top with three 6-W UV lamps with maximum emission at 365 nm (Philips F/TL/6 W/08, Holland). MO degradation was studied by UV–Vis spectroscopy following the variation in the intensity of the band at 508 nm with time up to 150 min. Results are represented as C/C_0 (%) versus irradiation time, where C_0 is the MO concentration at the starting point, and C is the MO concentration at time t. Photolysis and dark tests (adsorption) were performed to confirm that the degradation of MO is associated with the TiO_2 film activity, and not to light irradiation and/or adsorption.

3 Results and discussion

3.1 Characterisation of Ag nanoparticle colloidal suspensions

Aminosilane-stabilised silver nanoparticles (Ag-ATS) were obtained by colloidal synthesis. Figure 1a presents a TEM image of a dried drop of this suspension. The particles are spherical shaped with low aggregation and a particle size of 17 ± 4 nm (Fig. 1b). The particle size was also determined by light scattering arriving to a monomodal distribution centred at 21 ± 1 nm (Fig. 1c), in good agreement with TEM results. The colloidal suspension is yellow coloured and stable at room conditions for at least 30 days. The colour is likely due to the absorption of the local surface plasmon resonance (LSPR) typical of spherical metallic Ag nanoparticles [53]. UV–Vis spectra showed a typical absorption band in the visible range with a maximum at 406 nm (Fig. 2) associated with the presence of this LSPR.

PVP-stabilised silver nanoparticle colloidal suspension (Ag-PVP) also presents particles with spherical shape and size of 7 ± 2 nm with agglomerates of 45 nm (Fig. 3a). Light-scattering measurements show a narrow peak centred at 6 ± 1 nm (Fig. 3c), similar to the size measured from TEM images (Fig. 3b). Ag-PVP suspension was stable at room conditions and showed an orange colour with an intense absorption band at 402 nm in the UV–Vis spectrum (Fig. 2), also indicating the presence of LSPR.

XRD patterns of Ag-ATS and Ag-PVP suspensions deposited on Si wafers are shown in Fig. 4. For Ag-ATS, two peaks were identified, at $2\theta = 38.2°$ and 44.4°, and assigned to (111) and (200) planes, respectively, corresponding to face-centred cubic (fcc) Ag (JCPDS 04-0783). This confirms the presence of metallic Ag. For Ag-PVP, only the principal diffraction peak at $2\theta = 38.3°$ assigned to Ag-fcc was observed (Fig. 4b). The broad shape of the peak is likely due to the smaller size of the nanoparticles.

3.2 Characterisation of Ag-doped suspensions

Ag-doped SiO_2 and TiO_2 suspensions were obtained by mixing Ag-ATS or Ag-PVP colloidal suspensions with SiO_2 or TiO_2 sols, followed by solvent evaporation up to the final concentration. Ag-doped SiO_2 suspension was prepared adding Ag-ATS suspension dropwise to SiO_2 sol, obtaining a transparent, homogeneous, and orange sol. The more intense colour of Ag-doped SiO_2 sol with respect to the original suspension is associated with the higher concentration, and not with the increase in the Ag particle size. The UV–Vis absorption spectrum of Ag-doped SiO_2 suspension is very similar to that of the Ag-ATS one, not changing with the ageing time (Fig. 5a). This indicates that the metallic nanoparticles are not degraded (oxidised or dissolved) by the sol–gel medium. The initial viscosity of the Ag–SiO_2 sol was 2.5 mPa.s and remains constant for at least 1 month at room temperature. The condensation degree almost does not change for a considerable period, a very important aspect for future technological applications.

The Ag-doped TiO_2 suspensions were obtained by adding Ag-PVP colloidal suspension to TiO_2 and TiO_2-Brij58 sols; they are initially transparent, becoming translucent up to opaque with ageing time. The optical absorption spectra explain this behaviour (Fig. 5b, c). The peak at 406 nm decreases with the ageing time for both suspensions, indicating that the surface plasmon resonance of metallic Ag nanoparticles disappears, while a band at longer wavelength emerges during the first days of ageing. After some days, the peaks related to LSPR vanish (Fig. 5b, c), indicating that metallic silver nanoparticles are

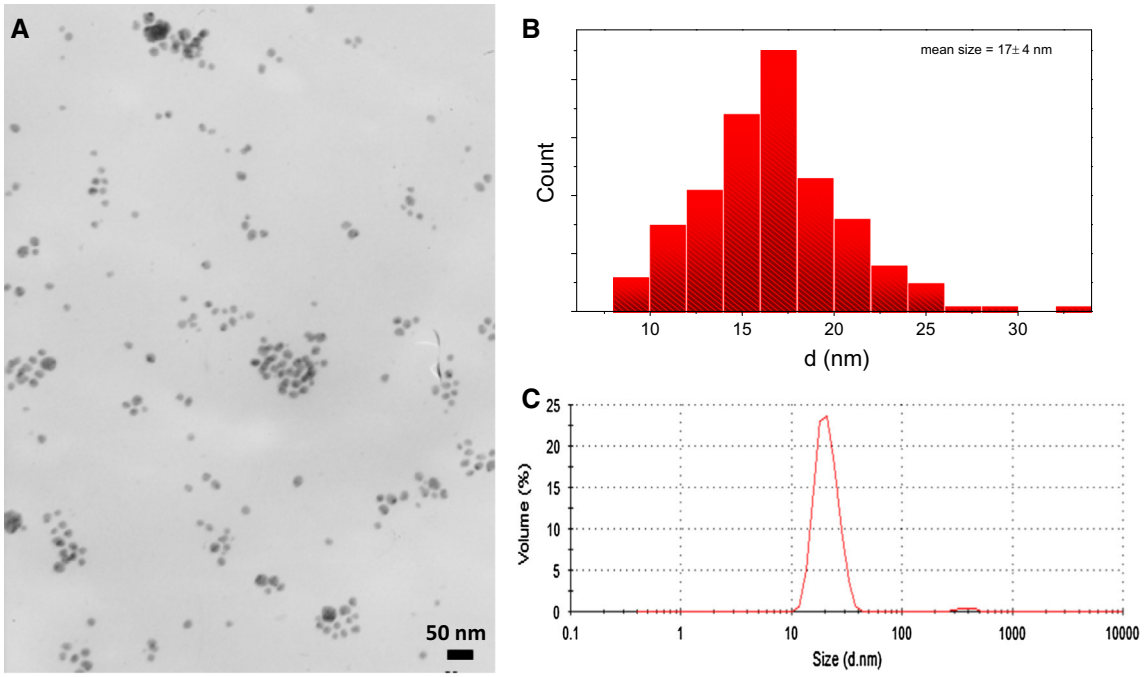

Fig. 1 Particle size of Ag-ATS NPs. **a** TEM image, **b** size distribution measured by TEM, and **c** size distribution obtained from light-scattering measurements

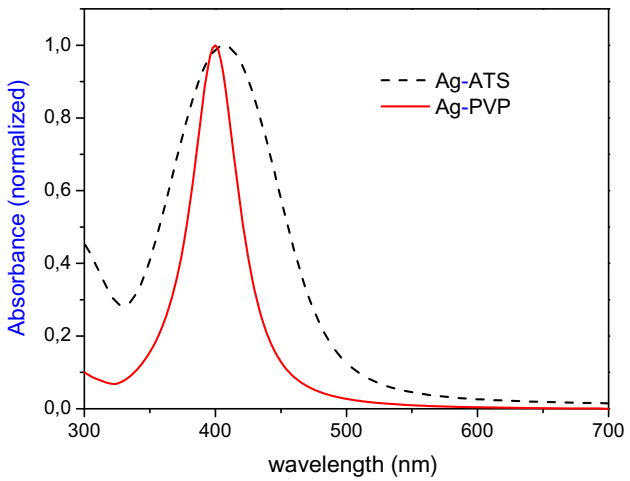

Fig. 2 UV–Vis spectra of Ag-ATS and Ag-PVP colloidal suspensions

partially oxidised when incorporated in the TiO_2 sol. On the other hand, the viscosity of the initial Ag-doped TiO_2 sols was 1.6 mPa.s and remains constant for at least 1 month.

To obtain experimental evidence of the Ag-NPs stability in the TiO_2 sol, GXRD patterns of dried Ag-doped TiO_2 suspensions deposited onto Si wafers were performed (Fig. 6). No diffraction peaks of metallic Ag^0 were found in both sols. All the peaks can be indexed as cubic AgCl (JCPDS 31-1238) at $2\theta = 27.9°$ (111); 32.3° (200); 46.4° (220); 55° (311); 57.8° (222). These results suggest the oxidation of metallic silver to Ag^+ in the TiO_2 sol and the subsequent formation of AgCl with Cl^- anions provided by HCl used as catalyst in the sol–gel synthesis.

3.3 Characterisation of doped coatings

$Ag–SiO_2$ and $Ag–TiO_2$ films were deposited by dipping onto Si wafers (heat treated at 450 °C) and characterised by FTIR analysis. The spectra (not shown) confirmed that the coatings are free of organic residues, and the only phase present is TiO_2 anatase (band at 435 cm^{-1}). FTIR spectrum of $Ag–SiO_2$ (not shown) film showed two bands at 447 and 1071 cm^{-1} corresponding to Si–O–Si vibrations.

The thickness and refractive index of the films deposited on glass slides were determined by spectral ellipsometry. Table 1 depicts the refractive index, thickness, and pore volume obtained by considering the BEMA model [57], at $\lambda = 700$ nm at room temperature in air. SiO_2 coatings were obtained with a thickness of $\approx$210 nm and a refractive index $\approx$1.44, close to dense material. $Ag–SiO_2$ coatings are thicker, about $\approx$380 nm, with a refractive index of 1.43. The thickness is enough in both cases to avoid the diffusion of Na^+ cations from the glass substrate to the TiO_2 coating during firing, thus preserving the semiconductor properties [59–61]. In the case of dense $Ag–TiO_2$ coatings, the addition of Ag-PVP causes an increase in thickness, from 90 to 290 nm and a simultaneous

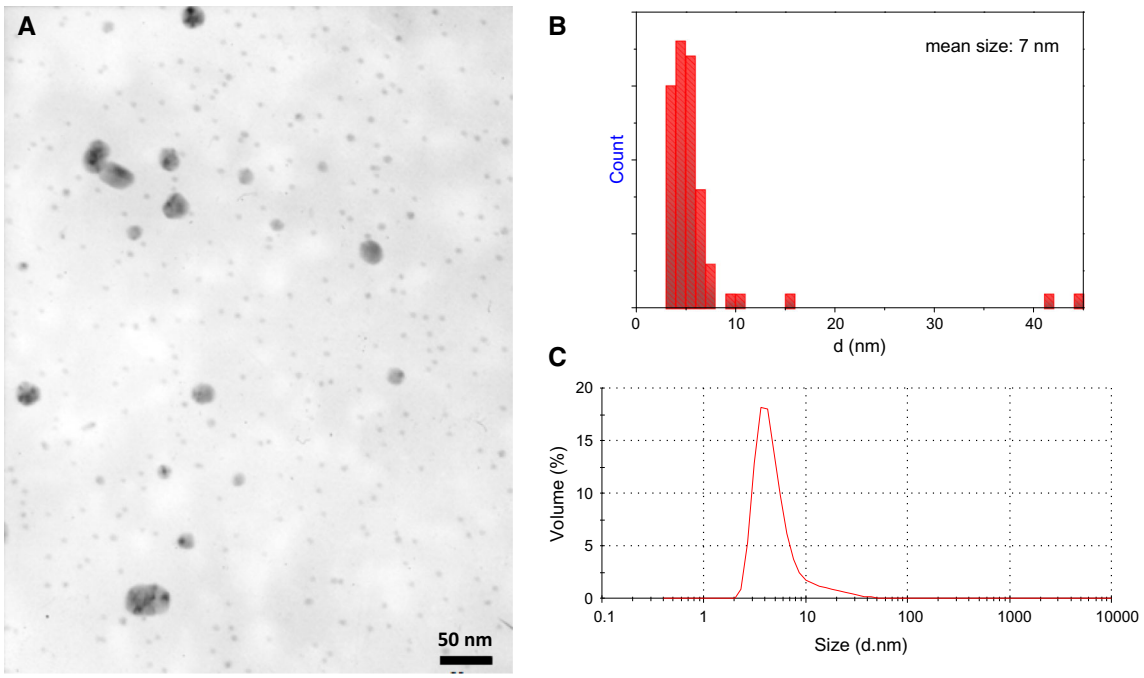

Fig. 3 Particle size of Ag-PVP NPs. **a** TEM image, **b** size distribution measured by TEM, and **c** size distribution by light scattering

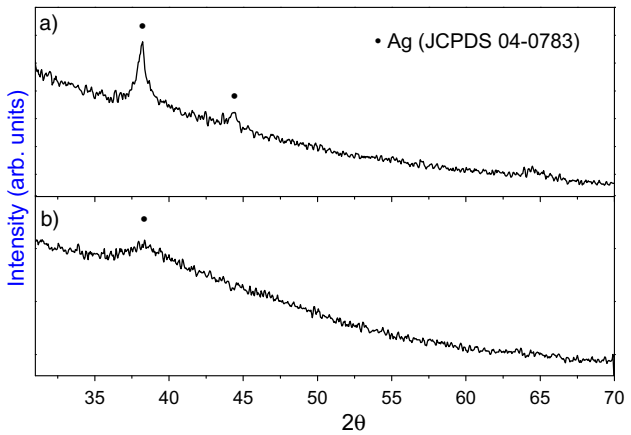

Fig. 4 GXRD of silver nanoparticle colloidal suspension dropped onto a Si substrate: **a** ATS-protected Ag nanoparticles and **b** PVP-protected Ag nanoparticles

decrease in the refractive index from 2.09 to 1.80, indicating the porous structure of the coating. The increase in the film thickness may be explained by the higher viscosity of the Ag-doped sol (1.6 Pa.s) versus the undoped sol (1.0 Pa.s), the presence of pores being revealed by the decreasing refractive index. The polymer used to stabilise the Ag-PVP suspension is eliminated during the film sintering, likely acting as pores agent.

The same effect is observed in the TiO_2 mesoporous coatings, where the incorporation of the surfactant Brij58 causes the decrease in refractive index and the increase in the film thickness. This effect is more evident in Ag–TiO_2 mesoporous coatings where both effects, surfactant (Brij58) and polymer stabiliser PVP, are combined.

Figure 7 shows the GXRD spectra of sintered Ag–SiO_2, dense Ag–TiO_2, and mesoporous Ag–TiO_2 films deposited onto Si wafers in the range $2\theta = 20°$–$70°$. For Ag–SiO_2 coatings, only one peak appears at $2\theta = 38.2°$, the main diffraction peak of metallic Ag, corresponding to the (111) plane diffraction of cubic fcc structure. Therefore, silver nanoparticles in SiO_2 films remain in the elemental metallic state (Ag^0) after the heat treatment. In the case of dense Ag–TiO_2 coating (Fig. 7b), different peaks of TiO_2 in anatase phase are identified (JCPDS-21-1272) at $2\theta = 25.35°$, $38.1°$, $48.1°$, $54.1°$, $55.15°$, $62.8°$. On the other hand, a broad peak at $2\theta = 38.1°$ could be associated with the overlapping of TiO_2 anatase and metallic Ag. The peak at 44.3° corresponding to the (200) diffraction plane of Ag-fcc appears as a smooth increase in the baseline. Other peaks appear at $2\theta = 32.3°$ and $37.1°$, attributed to (111) and (200) planes of Ag_2O (JCPDS-43-0997) and others at $2\theta = 27.8°$ and $32.2°$, assigned to AgCl (JCPDS 31-1238). Consequently, some reduction of Ag^+ to Ag^0 occurs during the heat treatment, although part of silver mainly remains as Ag^+.

In mesoporous Ag–TiO_2 film (Fig. 7c), anatase peaks are also identified, together with the metallic Ag-fcc (200) diffraction plane at $2\theta = 44.3°$, along with Ag_2O peaks at $2\theta = 32.1°$ and $37.1°$. The presence of metallic Ag indicates that ionic silver is partially reduced to metallic silver,

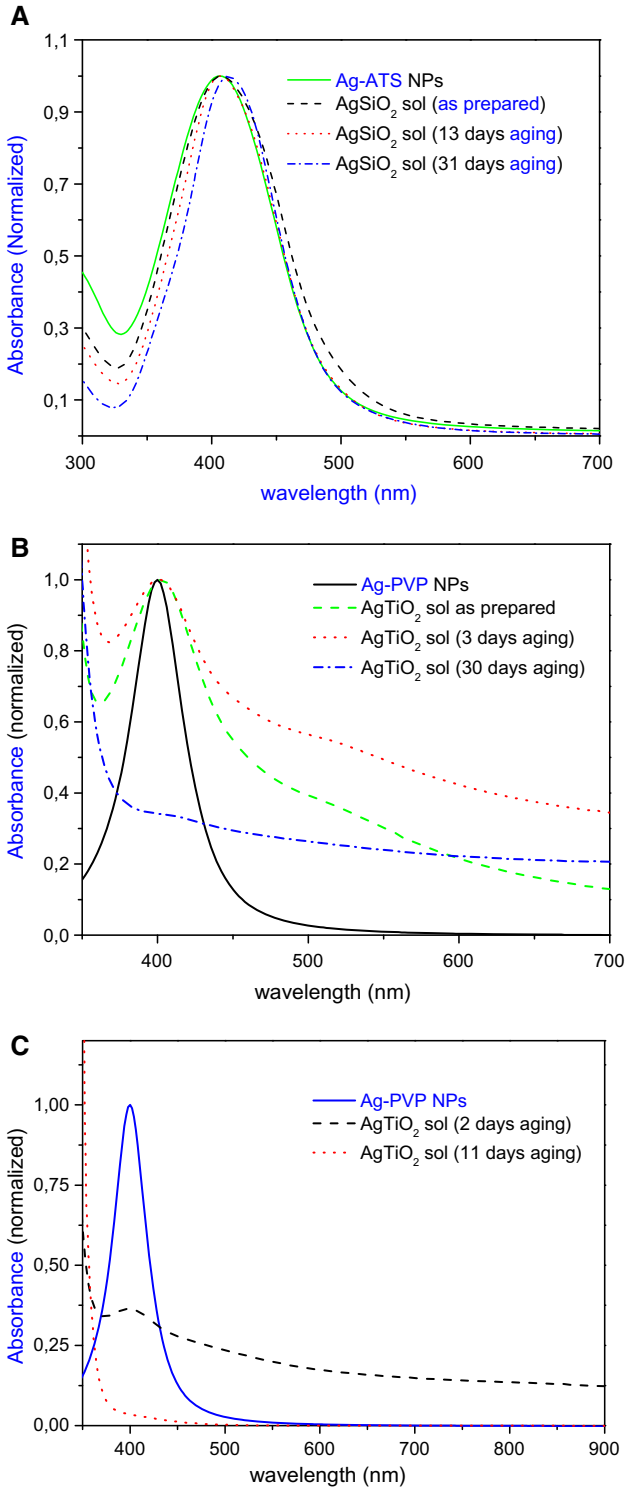

Fig. 5 UV–Vis spectra of silver colloidal nanoparticles and Ag-doped suspensions at different ageing times: **a** Ag-doped SiO_2 suspension, **b** Ag-doped dense TiO_2 suspension, and **c** Ag-doped TiO_2-Brij58 suspension

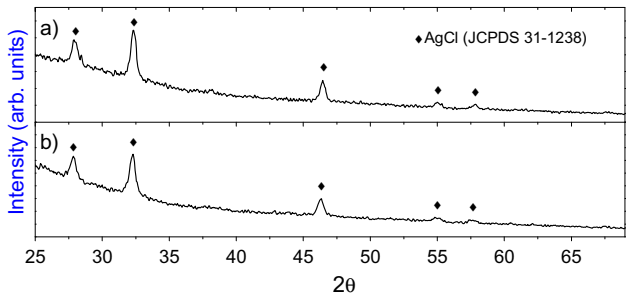

Fig. 6 GXRD of Ag-doped TiO_2 suspensions dropped onto a Si substrate: **a** Ag-doped dense TiO_2 suspensions, **b** Ag-doped TiO_2-Brij58 suspensions

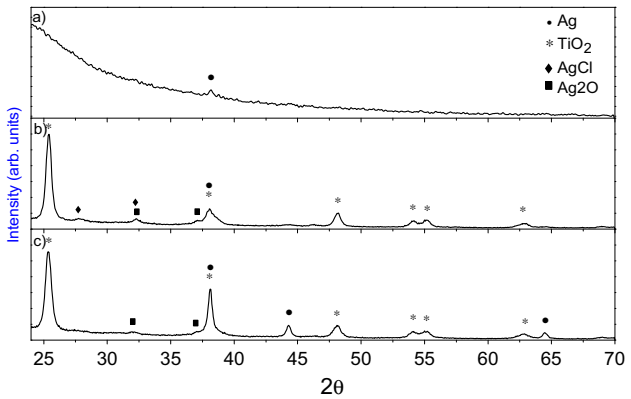

Fig. 7 GXRD patterns of Ag-doped films: **a** Ag-doped SiO_2 film; **b** Ag-doped dense TiO_2 film; **c** Ag-doped mesoporous TiO_2 film. Principal diffraction peaks are labelled

probably favoured by the presence of Brij58 organic compound during the heat treatment [30]. These results indicate that both suspensions (Ag-doped TiO_2 sol with and without Brij58) present a similar behaviour; however, after the heat treatment, the sol with Brij58 showed a higher concentration of metallic Ag-NPs, due to the most efficient reduction of Ag^+ to Ag^0. Thus, the surfactant seems to have a double benefit for improving the photocatalytic performance: it acts increasing the specific surface area and also allows obtaining higher concentration of metallic Ag-NPs.

Figure 8 shows TEM images of Ag–SiO_2, dense Ag–TiO_2, and Ag–TiO_2 mesoporous films. Ag–SiO_2 film (Fig. 8a) shows a dense coating with silver nanoparticle sizes around 10 ± 5 nm, near to the original size of Ag-ATS nanoparticle suspension (Fig. 1a, b, mean size $= 17 \pm 4$ nm). Thus, the silica matrix prevents the increase in particle size during the heat treatment. Ag–TiO_2 film (Fig. 8b) reveals a porous coating, according to ellipsometric data, likely generated by the polymer used to stabilise the Ag-PVP nanoparticles. Figure 8c shows a TEM image of Ag–mesoporous TiO_2 film with higher porosity. A quite uniform distribution of silver nanoparticles with particle size of 10 ± 4 nm is observed, indicating that the reduction process during the heat treatment

retrieves the original size of nanoparticles (Figs. 3a, b, mean size = 7 ± 2 nm).

3.4 Photocatalytic characterisation of Ag-doped coatings

The photocatalytic activity was studied through the degradation of MO in aqueous solution under UV illumination, using the multilayer systems described in Table 1 deposited on glass slides. The preliminary tests show that neither photolysis nor adsorption processes occur.

Figure 9a shows the decreasing curve of MO concentration versus time for Ag–SiO_2, SiO_2/TiO_2 dense, SiO_2/Ag–TiO_2 dense, and Ag–SiO_2/TiO_2 dense coatings, while Fig. 9b presents the results of SiO_2/TiO_2 meso, SiO_2/Ag–TiO_2 meso, and Ag–SiO_2/TiO_2 meso samples. The photocatalytic activity of Ag–SiO_2 coatings is negligible, indicating that Ag-NPs are not photocatalytically active (Fig. 9a). However, the combination of SiO_2 and TiO_2 coatings (Figs. 9a, b) presents photocatalytic activity for all the systems. SiO_2/TiO_2 dense coatings show an important degradation of MO, by decomposing the 58 % of MO after 2.5 h under UV irradiation. The photocatalytic activity increases with the incorporation of Ag nanoparticles to SiO_2 or TiO_2 coatings (Fig. 9a), demonstrating that the photodegradation reactions and the efficiency of the semiconductor are affected by the presence of Ag-NPs. Indeed, the SiO_2/Ag–TiO_2 dense coatings show a decomposition of 73 % of MO, while the Ag–SiO_2/TiO_2 dense system reaches a degradation of 86 % (Fig. 9a) in the same time. Additionally, the incorporation of the surfactant Brij58 causes a great improvement on the photocatalytic activity mainly due to the porous structure of the films and the increase in specific surface area (Fig. 9b). The degradation of MO increases from 58 to 67 % from SiO_2/TiO_2 dense to SiO_2/TiO_2 mesoporous coatings. The incorporation of Ag-NPs to SiO_2 or TiO_2 mesoporous coatings improves even more the efficiency of the semiconductor.

Between all the multilayered coatings described in this paper, the Ag–SiO_2/TiO_2 mesoporous coating system leads to the best photocatalytic effect with 94 % of MO degradation after 2.5 h, near the complete elimination of the pollutant. Afterwards, SiO_2/Ag–TiO_2 mesoporous coating system exhibits 86 % degradation after the same exposure time. The kinetic parameters of the photocatalytic decomposition of MO were reported in a previous work [51].

The increase in the photocatalytic activity can be explained considering several non-mutually exclusive mechanisms, by which metallic nanoparticles can enhance the rates of photocatalysis: (1) increase in the concentration of energetic reactive species by delaying the e–h recombination [62], (2) increase in the photon optical path length through TiO_2 by dispersion effects from NPs [63], (3) decrease in E_g by Ag-doping of TiO_2 [30], (4) increase in light intensity by LSPR and reinforcement of the near electric field [53, 64], and (5) increase in the contact surface between the catalytic material and the reaction medium [14, 26].

The electron transfer mechanism from TiO_2 to Ag-NPs increases the separation of e^-/h^+ pairs and avoids their recombination [32, 65]; thus, there is an increase in the pairs' lifetime that causes the increase in the concentration of reactive species, more holes being available to oxidise organic compounds as MO. This mechanism only acts when silver nanoparticles are in direct contact with TiO_2 semiconductor. To confirm that this mechanism is operating, photoluminescence measurements were taken. Photoluminescence signals are emitted when e^-/h^+ pairs in TiO_2 are recombined; if transference of e^- from the semiconductor to the metal occurs, the pair recombination is delayed, and photoluminescence intensity decreases. Figure 10 shows the photoluminescence spectra of SiO_2/TiO_2-doped and

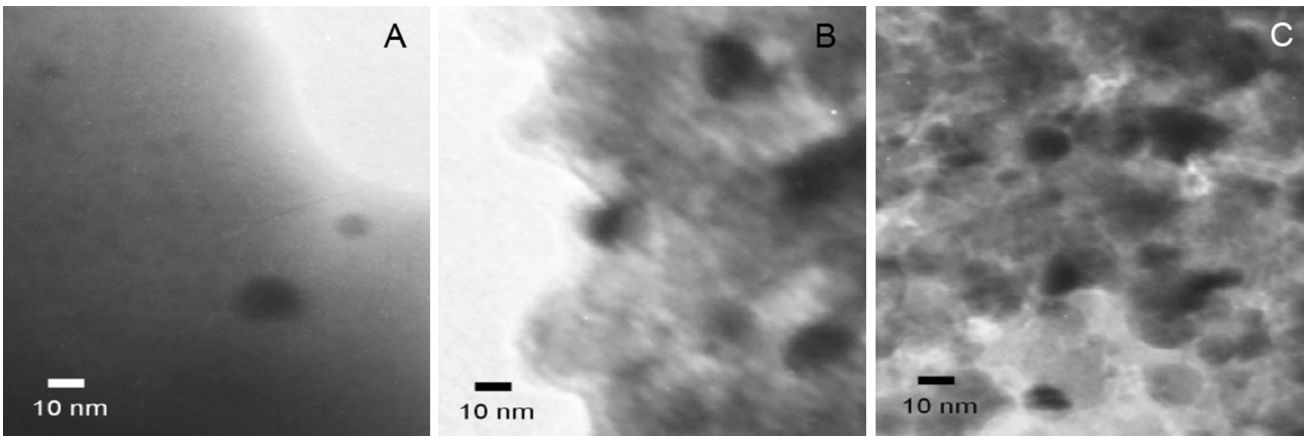

Fig. 8 TEM images of Ag-doped films: **a** Ag-doped SiO_2, **b** Ag-doped dense TiO_2, **c** Ag-doped mesoporous TiO_2 anatase

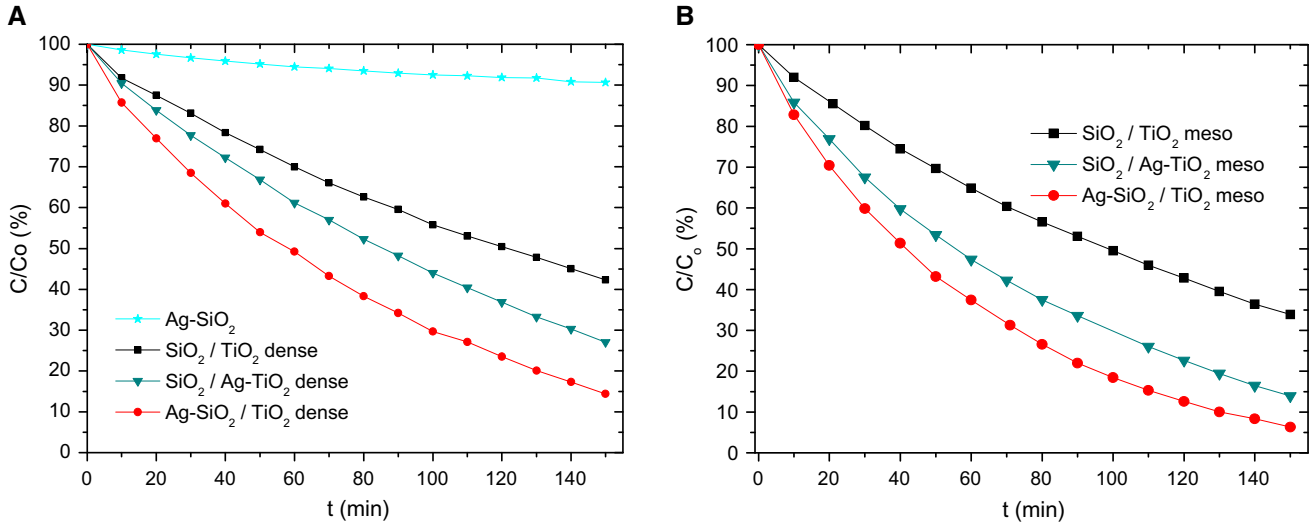

Fig. 9 Decomposition of methyl orange under UV irradiation as a function of time for all the coatings described in Table 1: **a** dense samples, **b** mesoporous samples

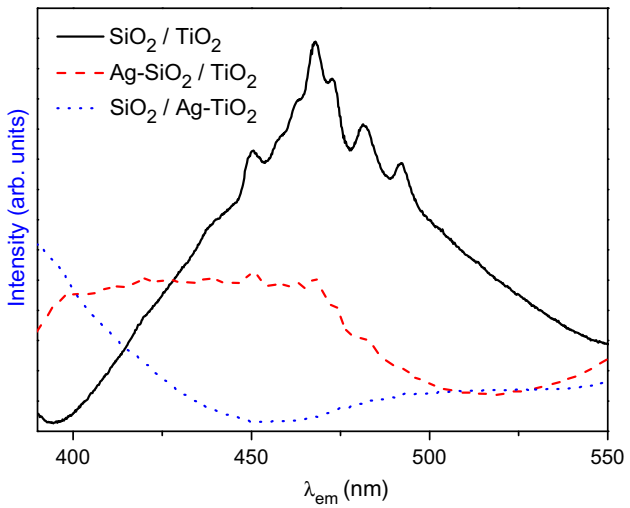

Fig. 10 Photoluminescence spectra of dense samples: SiO_2–TiO_2, Ag–SiO_2/TiO_2, and SiO_2/Ag–TiO_2

undoped dense coatings. The photoluminescence intensity decreases in Ag–SiO_2/TiO_2 dense sample with respect to the undoped sample, the emission being completely quenched in SiO_2/Ag–TiO_2 dense sample. These experiments show the transference of energetic photo-induced electrons from TiO_2 to Ag nanoparticles, this fact preventing the recombination of e^-/h^+ pairs. This effect is more important in the SiO_2/Ag–TiO_2 sample, where silver nanoparticles have an extensive interface with TiO_2. In Ag–SiO_2/TiO_2 system, only some silver nanoparticles on the top of SiO_2 layer are in contact with the semiconductor thus being less influenced by this mechanism. The same behaviour was observed in mesoporous samples [52].

The second possible mechanism involves the scattering of photons by nanoparticles, which increases the average photon path length through the composite. This mechanism is significant when nanoparticles are bigger than 50 nm, being negligible in samples with metal nanoparticles of 10 nm, as the present case. To disregard the action of this mechanism, UV–Vis transmission spectra of monolayers deposited onto quartz substrates were performed (Fig. 11a). From the comparison of doped and undoped coatings, it is observed that Ag-doped monolayers show a slight effect of scattering as a decrease in transmission towards shorter wavelengths. This effect is attributed to an increase in roughness, as shown by AFM images (Fig. 11b, c). All the Ag-doped coatings show higher roughness than the corresponding coating without silver (Table 1). In Fig. 11, it is clear that roughness increases for doping films, rising from 1.6 nm for dense SiO_2/TiO_2 system to 5.8 nm for dense SiO_2/Ag–TiO_2 samples. The increase in surface roughness may explain the higher dispersion effects and the consequent decrease in light transmission through the material [66, 67]. Thus, the occurrence of scattering effect is disregarded from both theoretical predictions and experimental results.

The third mechanism is related to band gap energy of TiO_2. Several authors reported that the incorporation of small amounts of metal nanoparticles could decrease the band gap energy of TiO_2 to the visible region, thus modifying the photocatalytic properties [68]. In order to study the effect of Ag-doping on TiO_2 films, E_g values were calculated from UV–Vis spectral data (Fig. 11) using the Eq. 1. For TiO_2 and Ag–TiO_2 mesoporous samples, values of 3.60 eV were obtained, whereas 3.50 eV for dense TiO_2 and 3.57 eV for dense Ag–TiO_2 were calculated.

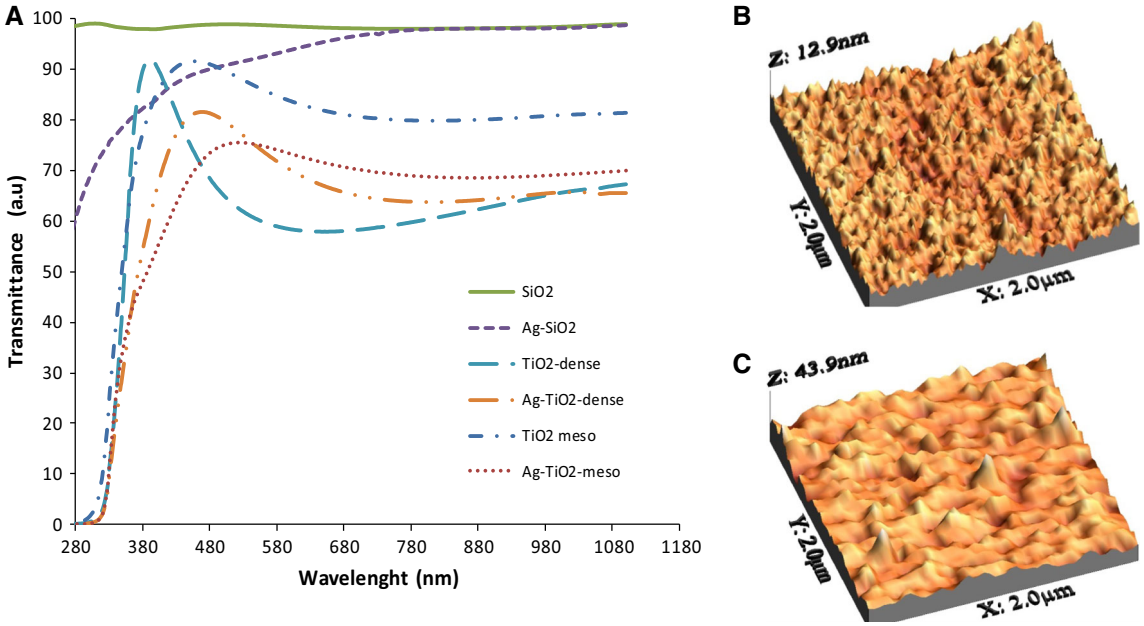

Fig. 11 **a** Transmittance spectra of monolayer coatings onto quartz substrates. AFM images of: **b** dense SiO_2/TiO_2 coatings and **c** dense SiO_2/Ag–TiO_2 coatings

Considering an error of 0.05 eV, the E_g values are near constant, no measurable decrease being introduced by Ag-doping effect. Indeed, this mechanism could not explain the different photocatalytic behaviour.

The fourth possible mechanism is associated with the excitation of the LSPR of silver nanoparticles. When LSPR occurs, strong electric fields are produced around the nanostructure. As the rate of electron–hole formation in a semiconductor is proportional to the local intensity of the electric field, the effect of LSPR could increase by a few orders of magnitude the electron–hole formation [64]. This mechanism could occur even if silver nanoparticles and TiO_2 are not in direct contact. During the synthesis of Ag-doped SiO_2 sol, Ag-ATS nanoparticles do not react with the SiO_2 sol, reflected in the stability of the LSPR absorption band after mixing both suspensions (Fig. 5a). GXRD diffractograms of these coatings (Fig. 7a) neither show any evidence of the presence of oxidised silver after heat treatment. On the other side, the partial oxidation of silver nanoparticles in the TiO_2 coatings acts decreasing the electric field associated with the LSPR effect and therefore decreases the possibility of enhancing the photocatalytic activity. The incorporation of metallic silver nanoparticles is more efficient in Ag–SiO_2 coatings than in Ag–TiO_2 coatings. The higher photocatalytic activity of Ag–SiO_2/TiO_2 system with respect to SiO_2/Ag–TiO_2 system could be explained by the presence of metallic Ag-NPs that reinforce the catalysis mechanism by near-field electromagnetic strengthening.

The last mechanism is related to the coating porosity. The highest photocatalytic efficiency was obtained for the Ag–SiO_2/TiO_2 mesoporous system and can be associated with the high porosity of titania coating (25 % v/v, calculated from ellipsometric data [57]) and the very good stability of silver nanoparticles during the entire preparation process. The porosity favours the migration of organic contaminants through the titania matrix.

In summary, homogeneous, transparent, and well-adhered photocatalytic films were prepared by sol–gel with different multilayer designs. In the case of Ag–SiO_2 matrix, the oxidation of Ag-NPs is prevented, and the metallic silver nanoparticles preserve the original redox state and size and are homogeneously distributed in the film. On the other hand, when colloidal silver nanoparticles are embedded into TiO_2 matrices, Ag-NPs easily react during synthesis and oxidation occurs, thus decreasing the concentration of metallic nanoparticles, resulting in a lower improvement of photocatalysis with respect to the system doped with the same concentration of Ag-NPs in the inner SiO_2 layer.

In this way, we have identified suitable synthesis conditions that allow obtaining a high reinforcement of the photocatalytic activity of SiO_2/TiO_2 coating systems. The most favourable strategy consists on the introduction of Ag-ATS NPs into the inner SiO_2 coating because the stability of the nanoparticles is maintained during the complete synthesis process. When silver nanoparticles are introduced into the TiO_2 layer, a partial oxidation of the

metallic nanoparticles occurs, and the load of active Ag^0 nanoparticles decreases. This phenomenon has been partially avoided using Brij58 as reducing agent, which also acts increasing the porosity and specific surface area.

4 Conclusions

Composite multilayered SiO_2/TiO_2 coatings doped with silver nanoparticles were obtained by sol–gel. SiO_2 sols doped with Ag-ATS nanoparticles are stable for a long time not affecting the redox state and size of the NPs. On the other side, TiO_2 sols provoke the partial oxidation of Ag^0 to Ag^+, this effect being lower when adding a reducing agent. The use of surfactant Brij58 allows achieving two benefits: the increase in the specific surface area of titania coatings and a higher amount of metallic Ag^0 nanoparticles. This demonstrates the important effect of the dispersion medium of silver NPs for preserving their oxidation state.

The different SiO_2/TiO_2 multilayer systems doped with Ag-NPs present improved photocatalytic activity. The highest efficiency among the photocatalytic systems was found to be: Ag–SiO_2/TiO_2 mesoporous > Ag–SiO_2/TiO_2 dense $\approx$ SiO_2/Ag–TiO_2 mesoporous coatings.

The formation of mesopores in the photoactive TiO_2 coating along with Ag-doping of the adjacent SiO_2 layer allowed obtaining the fastest organic degradation among all the studied coating systems. The results suggest that the stability of silver nanoparticles during the synthesis is a relevant fact that determines the final performance of the photocatalyst. These conclusions contribute to the available knowledge for the rational design of novel functional materials.

Acknowledgments V.R. acknowledges CONICET for the postdoctoral scholarship. The authors thank Antonio Tomás, Laura Peláez, and Aritz Iglesias for their assistance with the experimental techniques and Alejandro Olivieri for providing the spectrofluorophotometer.

References

1. Li J, Zhang J (2009) Optical properties and applications of hybrid semiconductor nanomaterials. Coord Chem Rev 253:3015–3041
2. Kamat PV, Vinodgopal K (1993) In: Ollis DF, Al-Ekabi H (eds) Photocatalytic purification and treatment of water and air. Elsevier Science, Amsterdam
3. Singh S, Mahalingam H, Singh P (2013) Polymer supported titanium dioxide photo-catalysts for environmental remediation. Appl Catal A Rev 462–463:178–195
4. Mansfield CM, Alloy MM, Hamilton J, Verbeck GF, Newton K, Klaine SJ, Roberts AP (2015) Photo-induced toxicity of titanium dioxide nanoparticles to Daphnia magna under natural sunlight. Chemosphere 120:206–210
5. Fujishima A, Hashimoto K, Watanabe K (1999) TiO_2 photocatalysis fundaments and applications. University of Tokyo Published by BKC, Inc., Chiyoda-ku
6. Pichat P, Disdier J, Hoang-van C, Mas D, Goutailler G, Gaysse C (2000) Purification/deodorization of indoor air and gaseous effluents by TiO_2 photocatalysis. Catal Today 63:363–369
7. Yao L, He J (2014) Recent progress in antireflection and self-cleaning technology—from surface engineering to functional surfaces. Prog Mater Sci 61:94–143
8. Chen J, Poon C (2009) Methods for air cleaning and protection of building occupants from airborne pathogens. Build Environ 44:1899–1906
9. Fujishima A, Zhang X, Tryk DA (2008) TiO_2 photocatalysis and related surface phenomena. Surf Sci Rep 63:515–582
10. Linsebigle A, Lu G, Yates J (1995) Photocatalysis on TiO_2 surfaces: principles, mechanisms, and selected results. Chem Rev 95:735–758
11. Nakajima A, Koizumi S, Watanabe T, Hashimoto K (2001) Effect of repeated photo-illumination on the wettability conversion of titanium dioxide. J Photochem Photobiol, A 146:129–132
12. Park H, Park Y, Kim W, Choi W (2013) Surface modification of TiO_2 photocatalyst for environmental applications. J Photochem Photobiol C: Photochem Rev 15:1–20
13. Okamoto K, Yamamoto Y, Tanaka H, Itaya A (1985) Kinetics of heterogeneous photocatalytic decomposition of phenol over anatase TiO_2 powder. Chem Soc Jpn 58:2015–2022
14. Arconada N, Castro Y, Durán A (2010) Photocatalytic properties in aqueous solution of porous TiO_2 anatase films prepared by sol–gel process. Appl Catal A 385:101–107
15. Padikkaparambil S, Yaakob Z, Narayanan BN, Ramakrishnan R, Viswanathan S (2012) Novel preparation method of nanosilver doped sol gel TiO_2 photocatalysts for dye pollutant degradation. J Sol-Gel Sci Technol 63:108–115
16. Bellantone M, Williams HD, Hench LL (2002) Broad-spectrum bactericidal activity of Ag_2O-doped bioactive glass. Antimicrob Agents Chemother 46:1940–1945
17. Chen H, Nanayakkara C, Grassian V (2012) Titanium dioxide photocatalysis in atmospheric chemistry. Chem Rev 112:5919–5948
18. Abou-Helal MO, Seeber WT (2002) Preparation of TiO_2 thin films by spray pyrolysis to be used as a photocatalyst. Appl Surf Sci 195:53–62
19. Wang X, Shi F, Gao X, Fanb C, Huang W, Feng X (2013) A sol–gel dip/spin coating method to prepare titanium oxide films. Thin Solid Films 548:34–39
20. Zheng SK, Wang TM, Xiang G, Wang C (2001) Photocatalytic activity of nanostructured TiO_2 thin films prepared by dc magnetron sputtering method. Vacuum 62:361–366
21. Lorenzetti M, Biglino D, Novak S, Kobe S (2014) Photoinduced properties of nanocrystalline TiO_2-anatase coating on Ti-based bone implants. Mater Sci Eng, C 37:390–398
22. Paily R, DasGupta A, DasGupta N (2002) Pulsed laser deposition of TiO_2 for MOS gate dielectric. Appl Surf Sci 187:297–304
23. Aarik J, Aidla A, Uustare T, Kuklib K, Sammelselgc V, Ritalad M, Leskelä M (2002) Atomic layer deposition of TiO_2 thin films from TiI_4 and H_2O. Appl Surf Sci 193:277–286
24. Byun D, Jin Y, Kim B, Lee JK, Park D (2000) Photocatalytic TiO(2) deposition by chemical vapor deposition. J Hazard Mater 73:199–206
25. Arabatzis IM, Antonaraki S, Stergiopoulos T, Hiskia A, Papaconstantinou E, Bernard MC, Falaras P (2002) Preparation, characterization and photocatalytic activity of nanocrystalline thin film TiO_2. J Photochem Photobiol A: Chem 149:237–245
26. Arconada N, Castro Y, Durán A, Héquet V (2011) Photocatalytic oxidation of methyl ethyl ketone over sol–gel mesoporous and

meso-structured TiO_2 films obtained by EISA method. Appl Catal B: Environ 107:52–58
27. Rayalua S, Josec D, Joshia M, Mangrulkara P, Shresthac K, Klabunde K (2014) Photocatalytic water splitting on Au/TiO_2 nanocomposites synthesized through various routes: Enhancement in photocatalytic activity due to SPR effect. Appl Catal B: Environ 142:684–693
28. Wang X, Fan H, Ren P (2013) Self-assemble flower-like SnO_2/Ag heterostructures: correlation among composition, structure and photocatalytic activity. Colloids Surf A: Phys Eng Asp 419:140–146
29. Zhao B, Chen Y (2011) Ag/TiO_2 sol prepared by a sol–gel method and its photocatalytic activity. J Phys Chem Solids 72:1312–1318
30. Ismail A (2012) Facile synthesis of mesoporous Ag-loaded TiO_2 thin film and its photocatalytic properties. Microporous Mesoporous Mater 149:69–75
31. Alem A, Sarpoolaky H (2010) The effect of silver doping on photocatalytic properties of titania multilayer membranes. Solid State Sci 12:1469–1472
32. McEvoy JG, Zhang Z (2014) Antimicrobial and photocatalytic disinfection mechanisms in silver-modified photocatalysts under dark and light conditions. J Photochem Photobiol Rev 19:62–75
33. Takai A, Kamat P (2011) Capture, store, and discharge. Shuttling photogenerated electrons across TiO_2–silver interface. ACS Nano 5:7369–7376
34. Bois L, Chassagneux F, Battie Y, Bessueille F, Mollet L, Parola S, Destouches N, Toulhoat N, Moncoffre N (2009) Chemical growth and photochromism of silver nanoparticles into a mesoporous titania template. Langmuir 26:1199–1206
35. Cai W, Zhong H, Zhag L (1998) Optical measurements of oxidation behavior of silver nanometer particle within pores of silica host. J Appl Phys 83:1705–1710
36. Li X, Lenhart J (2012) Aggregation and dissolution of silver nanoparticles in natural surface water. Environ Sci Technol 46:5378–5386
37. Akhavan O, Ghaderi E (2010) Self-accumulated Ag nanoparticles on mesoporous TiO_2 thin film with high bactericidal activities. Surf Coat Technol 204:3676–3683
38. Seery M, George R, Floris P, Pillai S (2007) Silver doped titanium dioxide nanomaterials for enhanced visible light photocatalysis. J Photochem Photobiol A: Chem 189:258–263
39. Rafiuddin ZZ (2012) Silver nanoparticles to self-assembled films: green synthesis and characterization. Colloids Surf B: Biointerfaces 90:48–52
40. Al-Ghamdi HS, Mahmoud WE (2013) One pot synthesis of multi-plasmonic shapes of silver nanoparticles. Mater Lett 105:62–64
41. Huang L, Zhai Y, Dong S, Wang J (2009) Efficient preparation of silver nanoplates assisted by non-polar solvents. J Colloid Interf Sci 331:384–388
42. Roldán MV, Scaffardi LB, de Sanctis OA, Pellegri NS (2008) Optical properties and extinction spectroscopy to characterize the synthesis of amine capped silver nanoparticles. Mater Chem Phys 112:984–990
43. Jeevanandam P, Srikanth C, Dixit S (2010) Synthesis of monodisperse silver nanoparticles and their self-assembly through simple thermal decomposition approach. Mater Chem Phys 122:402–407
44. Kotakadi V, Rao Y, Gaddam S, Prasad T, Reddy A, Gopal Sai (2013) Simple and rapid biosynthesis of stable silver nanoparticles using dried leaves of Catharanthus roseus. Linn. G. Donn and its anti-microbial activity. Colloids Surf B 105:194–198
45. Zhang D, Liu X, Wang X, Yang X, Lu L (2011) Optical properties of monodispersed silver nanoparticles produced via reverse micelle microemulsion. Phys B 406:1389–1394
46. Baek K, Kim J, Lee K, Ahnn H, Yoon C (2010) Surface plasmon resonance tuning of silver nanoparticle array produced by nanosphere lithography through ion etching and thermal annealing. J Nanosci Nanotechnol 10:3118–3122
47. Wadkar M, Chaudhari V, Haram S (2006) Synthesis and characterization of stable organosols of silver nanoparticles by electrochemical dissolution of silver in DMSO. J Phys Chem B 110:20889–20894
48. Roldán MV, de Sanctis O, Pellegri N (2013) Electrochemical method for Ag-PEG nanoparticles synthesis. J Nanoparticles 2013:524150–524157
49. Bordenave M, Scarpettini A, Roldán M, Pellegri N, Bragas A (2013) Plasmon-induced photochemical synthesis of silver triangular prisms and pentagonal bipyramids by illumination with light emitting diodes. Mater Chem Phys 139:100–106
50. Peng H, Yang A, Xiong J (2013) Green, microwave-assisted synthesis of silver nanoparticles using bamboo hemicelluloses and glucose in an aqueous medium. Carbohydr Polym 91: 348–355
51. Frattini A, Pellegri N, Nicastro D, de Sanctis O (2005) Effect of amine groups in the synthesis of Ag nanoparticles using aminosilanes. Mater Chem Phys 94:148–152
52. Roldán MV, de Oña P, Castro Y, Durán A, Faccendini P, Lagier C, Grau R, Pellegri N (2014) Photocatalytic and biocidal activities of novel coating systems of mesoporous and dense TiO_2-anatase containing silver nanoparticles. Mater Sci Eng, C 43:630–640
53. Kelly KL, Coronado E, Zhao LL, Schatz GC (2003) The optical properties of metal nanoparticles: the influence of size, shape, and dielectric environment. J Phys Chem B 107:668–677
54. Evanoff D, Chumanov G (2005) Synthesis and optical properties of silver nanoparticles and arrays. Chem Phys Chem 6: 1221–1231
55. Brinker CJ, Frye GC, Hurd AJ, Ashley CS (1997) Fundamentals of sol–gel dip coating. Thin Solid Films 201:97–108
56. Nam H, Amemiya T, Murabayashi M, Itoh K (2004) Photocatalytic activity of sol–gel TiO_2 thin films on various kinds of glass substrates: the effects of Na^+ and primary particle size. J Phys Chem B 108:8254–8259
57. Boissiere C, Grosso D, Lepoutre S, Nicole L, Bruneau AB, Sanchez C (2005) Porosity and mechanical properties of mesoporous thin films assessed by environmental ellipsometric porosimetry. Langmuir 21:12362–12371
58. Martínez S, Serrano T, Gómez I, Hernández A (2007) Síntesis y caracterización de nanoparticulas de CdS obtenidas por Microondas. Bol Soc Esp Ceram Vidr 46:97–101
59. Fernández A, Lassaletta G, Jiménez VM, Justo A, González-Elipe A, Herrmann JM, Tahiri H, Ait-Ichou Y (1995) Preparation and characterization of TiO_2 photocatalysts supported on various rigid supports (glass, quartz and stainless steel). Comparative studies of photocatalytic activity in water purification. Appl Catal B: Environ 7:49–63
60. Nocuń M, Burcon D, Siwulski S (2008) Sodium diffusion barrier coatings prepared by sol–gel method. Opt Appl XXXVIII: 172–179
61. Novotna P, Krysa J, Maixner J, Kluson P, Novak P (2010) Photocatalytic activity of sol–gel TiO_2 thin films deposited on soda lime glass and soda lime glass precoated with a SiO_2 layer. Surf Coat Technol 204:2570–2575
62. Shi J, Chen J, Feng Z, Lian Y, Wang X, Li C (2007) Photoluminescence characteristics of TiO_2 and their relationship to the photoassisted reaction of water/methanol mixture. J Phys Chem C 111:693–699
63. Linic S, Christopher P, Ingram DB (2011) Plasmonic-metal nanostructures for efficient conversion of solar to chemical energy. Nat Mater 10:911–921

64. Awazu K, Fujimaki M, Rockstuhl C, Tominaga J, Murakami H, Ohki Y, Yoshida N, Watanabe T (2009) A plasmonic photocatalyst consisting of silver nanoparticles embedded in titanium dioxide. J Am Chem Soc 130:1676–1680
65. Furube A, Du L, Hara K, Katoh R, Tachiya M (2007) Ultrafast plasmon-induced electron transfer from gold nanodots into TiO_2 nanoparticle. J Am Ceram Soc 129:14852–14853
66. Naceur BJ, Gaidi M, Bousbih F, Mechiakh R, Chtourou R (2012) Annealing effects on microstructural and optical properties of nanostructured-TiO_2 thin films prepared by sol–gel technique. Curr Appl Phys 12:422–428
67. Bose R, Kumar R, Sudheer S, Reddy V, Ganesan V, Pillai V (2012) Effect of silver incorporation in phase formation and band gap tuning of tungsten oxide thin film. J Appl Phys 112: 114311–114319
68. Lalueza P, Monzon M, Arruebo M, Santamaría J (2011) Bactericidal effects of different silver-containing materials. Mater Res Bull 46:2070–2076